CHILEAN JOURNAL of AGRICULTURAL RESEARCH
RESEARCH ARTICLE

Plant electrophysiological characteristics reveal the leaf intracellular nutrient metabolism and stress tolerance underlying Se(IV)-mediated alleviation of polyethylene stress in *Plantago asiatica*

Hanqing Meng[1], Xiongfei Cai[1], Ji Wang[1*], Antong Xia[2*], Yanyou Wu[3*], Juke Zhang[3], Jing Fan[2, 4], Kun Zhai[2, 4], and Dongshan Xiang[2, 4]

[1]Guizhou Normal University, School of Geography and Environmental Sciences, Guiyang, Guizhou 550025, China.
[2]Hubei Minzu University, School of Chemical and Environmental Engineering, Enshi, China.
[3]Institute of Geochemistry, Chinese Academy of Sciences, Guiyang, Guizhou, China.
[4]Hubei Minzu University, Hubei Key Laboratory of Selenium Resource Research and Biological Application, Enshi, China.
[*]Corresponding authors (wangji@gznu.edu.cn, antonexiaucas@yeah.net, wuyanyou@mail.gyig.ac.cn)
Received: 10 November 2025; Accepted: 9 March 2026, doi:10.4067/S0718-58392026000300472

ABSTRACT

Leaf intracellular nutrient metabolism plays a critical role in determining plant stress tolerance. Selenium(IV) supplied as sodium selenite (Na_2SeO_3; SeO_3^{2-}) has been reported to enhance plant resistance to polyethylene (PE, microplastics), yet its effects on intracellular nutrient metabolism under PE stress remain unclear. Plantain (*Plantago asiatica* L.) was exposed to PE (1500 mg kg^{-1}) and supplemented with Se(IV) at 0, 1.25, 2.5, 12.5, and 25 mg kg^{-1} (as Na_2SeO_3). Growth traits, photosynthetic performance, and leaf electrophysiological characteristics were measured, and the membership function method was used to comprehensively evaluate intracellular water-holding capacity (IWHC), nutrient transport capacity (NTC), and metabolic activity (MA). The Se(IV) dose 2.5 mg kg^{-1} produced the strongest overall mitigation of PE stress, increasing IWHC and MA by 173.95% and 24.70%, respectively, while maintaining a high NTC (129.69% above the PE-only treatment). When Se(IV) exceeded 2.5 mg kg^{-1}, mitigation weakened: At 12.5 and 25 mg kg^{-1}, IWHC, NTC, and MA increased by 77.01%, 105.01%, and 2.24%, and by 89.06%, 105.31%, and 16.22%, respectively, compared with the PE-only treatment, indicating that excess Se(IV) did not further improve plant performance. Overall, plant electrophysiological techniques provide a rapid and non-destructive approach to evaluate Se-mediated alleviation of microplastic stress and support the rational use of Se in agriculture.

Key words: Electrophysiological characteristics, intracellular nutrient metabolism, *Plantago asiatica*, polyethylene stress, selenium(IV) (sodium selenite).

INTRODUCTION

Polyethylene (PE, microplastic particles smaller than 5 mm) pollution refers to contamination caused by PE resin granules that persist in the environment, posing significant threats to soil health and human well-being (Li et al., 2022). Reports indicate that untreated PE waste in China alone could reach up to 4.4 billion tons annually, representing a major risk to agricultural productivity both domestically and globally (Qiu et al., 2023). Soil PE pollution directly harms plants by inhibiting nutrient metabolism, reducing the uptake of water, N, and other essential nutrients (Rajput et al., 2021); impairing growth, which leads to decreases in biomass and photosynthetic efficiency (Qiu et al., 2023); and damaging chloroplast structure, which exacerbates PE

toxicity (Li et al., 2022). Consequently, mitigating plant stress from PE is critical for effectively addressing global PE pollution.

Selenium(IV), supplied as sodium selenite (Na_2SeO_3; SeO_3^{2-}), can alleviate PE-induced stress by protecting chloroplast structure and mitigating oxidative damage caused by reactive oxygen species (ROS) (Shah et al., 2024); promoting the accumulation of osmolytes like proline and soluble sugars to reduce intracellular water loss (Bhadwal and Sharma, 2022); and enhancing the expression of key genes such as nitrate reductase (NR), channel protein (AKT1), and exchanger (CAX), which facilitate nutrient ion uptake (N, K, Ca) (Yuan et al., 2024), thereby enhancing plant stress tolerance. However, Se(IV) is not a macronutrient for plants, and excessive Se(IV) may lead to toxicity and inhibit plant growth (Hasanuzzaman et al., 2022). Therefore, identifying the optimal Se(IV) concentration for alleviating PE stress is crucial.

Leaf nutrient metabolism plays a pivotal role in plant stress tolerance, involving Se(IV) supplied as sodium selenite (Na_2SeO_3; SeO_3^{2-}): Reduction and assimilation, osmotic adjustment, and activation of stress signaling pathways. The reduction product of Se(IV), selenodiglutathione (GS-Se-CG), scavenges ROS in leaves (Hasanuzzaman et al., 2020). Within chloroplasts, selenomethionine (SeMet), an assimilation product of Se(IV), enhances the activity of Rubisco, thereby improving photosynthesis (Hasanuzzaman et al., 2020). Se(IV) can also stimulate expression of the proline biosynthesis gene *P5CS* in tomato leaves, increasing proline and soluble sugars and improving leaf water status (Bhadwal and Sharma, 2022). In addition, selenite upregulates metallothionein (MT) and phytochelatin synthase (PCS), contributing to heavy-metal tolerance (Brown et al., 2022). These processes depend on transmembrane transport of Se(IV) and its metabolites across the leaf cell membrane.

Plant electrical signals are continuously associated with metabolic processes, and the transmembrane transport of nutrient ions across the leaf cell membrane induces changes in leaf electrical signaling (Kulbacka et al., 2018). For instance, abiotic stress triggers the directional migration of K^+ and Ca^{2+} across the cell membrane, altering the transmembrane potential gradient and eliciting differential responses in plant electrical signals (Li et al., 2021). Consequently, previous research has inferred the characteristics of nutrient-ion transport within leaves and examined how plant growth responds to various stresses by tracking stress-induced changes in leaf electrical signals. Traditional electrophysiological methods, such as the puncture method, electrode method, and electrode plate method (Liu et al., 2018; Jócsák et al., 2019), are commonly employed to acquire leaf electrical signals and assess their environmental responses. However, these methods have significant limitations. First, they are destructive; obtaining plant electrical signals requires damaging plant tissues. Second, they provide only basic electrical readouts—such as resistance (R), impedance (Z), and inductance (L)—and do not accurately quantify electrophysiological attributes, including intracellular water metabolism, nutrient transport, and cellular metabolic energy. Thus, earlier electrophysiological techniques have neither elucidated the mechanisms of leaf electrophysiological nutrient metabolism nor identified electrophysiological indices of plant stress tolerance.

Fortunately, recent advancements by our team have led to the development of a model for plant electrophysiological characteristics that addresses these issues. The process involves the following steps: Initially, physicochemical kinetic equations between conventional plant electrical signals and different fixed clamping forces are established, which allow us to obtain the intrinsic electrophysiological properties of leaves at zero clamping force—i.e., under natural conditions—such as intrinsic capacitance, resistance, impedance, physiological capacitive reactance, and physiological inductive reactance. Next, an electrochemical absorption kinetics equation was constructed based on these intrinsic electrophysiological properties to calculate leaf intracellular nutrient metabolism features. These include parameters for intracellular water metabolism: Intracellular water-holding capacity (IWHC), intracellular water-use efficiency (IWUE), intracellular water-holding time (IWHT), and water transfer rate (WTR); as well as parameters for intracellular nutrient translocation: Nutrient flux per unit area (UNF), nutrient transfer rate (NTR), nutrient translocation capacity (NTC), active nutrient transport flow (UAF), and nutrient active translocation capacity (NAC). Additionally, using these leaf intracellular nutrient parameters, cellular metabolic energy and relative metabolic flow (Qin et al., 2022) are further quantified, all of which are key parameters of leaf intracellular nutrient metabolism.

The plant electrophysiological technology has been widely applied for online monitoring of growth responses of rice, Chinese cabbage, and potato to environmental stress (Zhang et al., 2020; 2021). Plantain

(*Plantago asiatica* L.), a remediation plant commonly used to mitigate soil microplastic pollution and intercept microplastics in aquatic environments, effectively reduces the environmental risks posed by microplastics (Li et al., 2021). In the present study, *P. asiatica* was chosen as the experimental plant. Using growth traits, photosynthesis, and leaf electrophysiology-derived intracellular nutrient metabolism features—including intracellular water metabolism, nutrient translocation, cellular metabolic energy, and metabolic flow—this study employed the membership function method to screen electrophysiological indicators and clarify the leaf intracellular nutrient metabolism features and stress tolerance mechanisms through which Se(IV) (sodium selenite) mitigates PE stress in *P. asiatica*. This study aimed to address the following questions: (1) To quantify the leaf intracellular nutrient metabolism features by which Se(IV) alleviates in *P. asiatica* using plant electrophysiological methods; and (2) to screen stress-resistance indices based on the membership function method and identify the optimal Se(IV) concentration for improving PE tolerance in *P. asiatica*.

MATERIALS AND METHODS

Culture of plants

The experimental material was *Plantago asiatica* L. cultivated indoors in pots. Healthy seeds were selected and sown in seedling trays containing a 2:1 mixture of perlite and vermiculite. Seedlings were grown under root-irrigation cultivation with half-strength Hoagland nutrient solution for 3-4 wk. Uniform plants were then transplanted into plastic pots (diameter 23 cm, height 16.5 cm), with 2 kg substrate per pot. Five independent pots were set up, each containing six plants. Environmental conditions were maintained at 25 ± 1 °C, 60 ± 5% humidity, 12:12 h photoperiod (Zhang et al., 2020), and a light intensity of 500 µmol m^{-2} s^{-1} (photosynthetic photon flux density, PPFD). The Hoagland nutrient solution was adjusted to pH 7.0 and replaced every other day, with the volume replenished to 2 L per pot at each change.

Polyethylene (PE) and Se(IV) (sodium selenite) treatments

Table 1 and Figure 1 summarize the polyethylene (PE) and Se treatments. The PE concentration was 1500 mg kg^{-1} (Chang et al., 2019). Selenium was supplied as sodium selenite (Na_2SeO_3; SeO_3^{2-}, analytical grade) (Chang et al., 2019). Microplastics were PE particles mixed into the substrate (1000-mesh fragments) (Qiu et al., 2023).

Table 1. Polyethylene (PE) and treatment of *Plantago asiatica* with different Se(IV) (sodium selenite) concentrations.

CK	0 mg kg^{-1} Se(IV) + 1500 mg kg^{-1} PE
S1	1.25 mg kg^{-1} Se(IV) + 1500 mg kg^{-1} PE
S2	2.5 mg kg^{-1} Se(IV) + 1500 mg kg^{-1} PE
S3	12.5 mg kg^{-1} Se(IV) + 1500 mg kg^{-1} PE
S4	25 mg kg^{-1} Se(IV) + 1500 mg kg^{-1} PE

Figure 1. *Plantago asiatica* samples: 0 mg kg^{-1} Se(IV) (CK); PE-1500 mg kg^{-1} (a); S1: 1.25 mg kg^{-1} Se(IV); PE-1500 mg kg^{-1} (b); S2: 2.5 mg kg^{-1} Se(IV); PE-1500 mg kg^{-1} (c); S3: 12.5 mg kg^{-1} Se(IV); PE-1500 mg kg^{-1} (d); S4: 25 mg kg^{-1} Se(IV); PE-1500 mg kg^{-1} (e). Se(IV): Selenium(IV) supplied as sodium selenite (Na_2SeO_3; SeO_3^{2-}); PE: polyethylene.

Growth characteristics and photosynthesis

In this experiment, the second or third fully expanded leaf of *P. asiatica* was selected. Crown width (Crown) and plant height (Height) were measured with a vernier caliper (YBCK-01, China). Leaf total chlorophyll content (TChl) and total N content (TN) were determined using a chlorophyll meter (TYS-4N, Sanli Grain Sorting Machinery, Shijiazhuang, Hebei, China). Three replicate measurements were taken for each leaf (Zhang et al., 2021).

As above, under illuminated conditions the second or third fully expanded leaf of *P. asiatica* was selected. A LI-6400 portable photosynthesis system (LI-COR Biosciences, Lincoln, Nebraska, USA) was used to measure net photosynthetic rate (P_N), stomatal conductance (g_{sw}), intercellular CO_2 concentration (C_i), and transpiration rate (T_r). For each leaf, three replicate datasets were obtained, with five readings per replicate. Water-use efficiency (WUE) was calculated according to Equation 1 (Zhang et al., 2020; 2021):

$$\mathrm{WUE} = \mathrm{P_N}/\mathrm{T_r} \qquad (1)$$

Determination of plant electrophysiological information

For electrophysiological testing, leaves were selected from uniformly grown plants, and electrophysiological information was measured using the parallel-plate capacitor. For each treatment, the third, fourth, and fifth fully expanded leaves were measured. Fresh leaves were soaked for 30 min, surface moisture was gently removed, and samples were prepared for measurement. Leaves were clamped between the parallel plates; measurement voltage and frequency were set to 1.5 V and 3000 Hz, respectively. The parallel-plate capacitive sensor was connected to an LCR meter and, in parallel mode, leaf physiological capacitance (C), physiological resistance (R), and physiological impedance (Z) were recorded under different clamping forces (F = 1, 2, 3, 5, and 7 N). In total, 15 datasets were used for fitting.

To minimize measurement perturbation and obtain intrinsic leaf electrophysiological information, the relationships between clamping force (F) and measured electrical parameters were fitted and extrapolated to F = 0 (Zhang et al., 2020; 2021). The corresponding equations are given below, and all symbols are defined after

the equations.

$$C = y_0 + aF \quad (2)$$

$$R = y_1 + a_1 e^{-b_1 F} \quad (3)$$

$$Z = y_2 + a_2 e^{-b_2 F} \quad (4)$$

The capacitive reactance $X_C(F)$ was calculated from capacitance:

$$Xc(F) = \frac{1}{2\pi f C(F)} \quad (5)$$

The inductive reactance $X_L(F)$ was calculated from R(F), Z(F), and XC(F) as:

$$\frac{1}{X_L(F)} = \frac{1}{Z(F)} - \frac{1}{R(F)} - \frac{1}{Xc(F)} \quad (6)$$

Intrinsic (i.e., minimally perturbed) electrophysiological parameters were obtained by extrapolation to F = 0:

$$ICP = C(0), IR = R(0), IZ = Z(0), IX_C = X_C(0), IX_L = X_L(0) \quad (7)$$

where C(F), R(F), and Z(F) are the leaf physiological capacitance, resistance, and impedance measured under clamping force F(N), respectively; F is the test frequency (3000 Hz); $X_C(F)$ and $X_L(F)$ are the capacitive and inductive reactance under clamping force F, respectively; ICP, IR, IZ, IX_C, and IX_L are the intrinsic capacitance, intrinsic resistance, intrinsic impedance, intrinsic capacitive reactance, and intrinsic inductive reactance obtained at F = 0, respectively; and y_0, y_1, y_2, a, a_1, a_2, b_1, and b_2 are fitted constants.

Intracellular water metabolism based on plant electrophysiological characteristics

Intracellular water-metabolism indices were calculated from intrinsic electrophysiological parameters (obtained at F = 0) following Zhang et al. (2020; 2021). The intrinsic water conductivity (IWC) was calculated as:

$$IWC = \frac{0.5hf}{1000} \quad (8)$$

Intracellular water-holding capacity (IWHC) was calculated from intrinsic physiological capacitance (ICP) as:

$$IWHC = \sqrt{(ICp)^3} \quad (9)$$

Leaf-specific effective thickness (d) was calculated as:

$$d = \frac{U^2 h}{2} \quad (10)$$

Intracellular water-use efficiency (IWUE) was calculated as:

$$IWUE = \frac{d}{IWHC} \quad (11)$$

Plant relative water-holding time (IWHT) was calculated using intrinsic capacitive reactance and intrinsic impedance as:

$$IWHT = ICP \times IZ \quad (12)$$

Leaf dynamic water-transfer rate (WTR) was calculated as:

$$WTR = \frac{IWHC}{IWHT} \quad (13)$$

where IWC is intrinsic water conductivity; IWHC is intracellular water-holding capacity; d is leaf-specific effective thickness; IWUE is intracellular water-use efficiency; IWHT is relative water-holding time; WTR is dynamic water-transfer rate; h is a fitted constant obtained from the C(F) fitting in the previous subsection; f is the test frequency (3000 Hz); U is the measurement voltage (1.5 V); ICP = C(0) is intrinsic physiological capacitance; $IX_C = X_C(0)$ is intrinsic capacitive reactance; and IZ = Z(0) is intrinsic impedance.

Nutrient transport characteristics based on plant electrophysiological characteristics

Plant cells exhibit capacitive and inductive electrical characteristics because the cell membrane functions as a dielectric layer containing embedded proteins and ion-transport pathways. Nutrient-transport indices were derived from intrinsic electrophysiological parameters (obtained at F = 0) following Zhang et al. (2020; 2021).

The nutrient unit flow (UNF) was calculated as:

$$UNF = \frac{R}{Xc} + \frac{R}{XL} \quad (14)$$

In this framework, the nutrient translocation rate (NTR) was assumed to equal the water-transfer rate (WTR):

$$NTR = WTR \quad (15)$$

Nutrient translocation capacity (NTC) was calculated as:

$$NTC = UNF \times NTR \quad (16)$$

The active transport flow of nutrients (UAF) was calculated as:

$$\mathrm{UAF} = \frac{\mathrm{Xc}}{\mathrm{XL}} \quad (17)$$

Nutrient active translocation capacity (NAC) was calculated as:

$$\mathrm{NAC} = \mathrm{UAF} \times \mathrm{NTR} \quad (18)$$

where UNF is nutrient unit flow; NTR is nutrient translocation rate; NTC is nutrient translocation capacity; UAF is active transport flow of nutrients; NAC is nutrient active translocation capacity; and R, X_C, and X_L are intrinsic physiological resistance, intrinsic capacitive reactance, and intrinsic inductive reactance (i.e., IR, IX_C, and IX_L) obtained at F = 0, respectively.

Cellular metabolic energy based on leaf electrophysiological characteristics

Leaf cellular metabolic-energy indices were calculated from intrinsic electrophysiological parameters following Zhang et al. (2020; 2021). Intermediate terms were defined as:

$$\Delta G_{LR-E} = \frac{\ln k_1 - \ln y_0}{b_1} \quad (19)$$

$$\Delta G_{LZ-E} = \frac{\ln k_2 - \ln \mathrm{p}_0}{b_2} \quad (20)$$

$$\Delta G_{LE} = \frac{\Delta G_{LR-E} + \Delta G_{LZ-E}}{2} \quad (21)$$

Leaf total cellular metabolic energy based on intrinsic resistance and intrinsic impedance was calculated as:

$$\Delta GL_R = \Delta G_{R-E} d \quad (22)$$

$$\Delta G_{LZ} = \Delta G_{Z-E} d \quad (23)$$

$$\Delta GL = \frac{\Delta G_R + \Delta G_Z}{2} \quad (24)$$

where ΔG_{LR-E} and ΔG_{LZ-E} are intermediate energy-related terms derived from the fitted models of intrinsic resistance and intrinsic impedance, respectively; ΔG_{LE} is the averaged intermediate term; ΔG_{LR} and ΔG_{LZ} are leaf total cellular metabolic energy components based on intrinsic resistance and intrinsic impedance, respectively; and ΔG_L is the overall leaf total cellular metabolic energy. y_0 and p_0 are fitted constants (intercepts) from the corresponding fitted models; b_1 and b_2 are fitted decay constants; k_1 and k_2 are fitted constants (scaling factors); and d is leaf-specific effective thickness calculated in Equation 10.

Metabolic flow based on electrophysiological characteristics of plant leaves

Metabolic flow indices were calculated from intrinsic electrophysiological parameters (obtained at F = 0) following Zhang et al. (2020; 2021). The metabolic flow (MF), metabolic rate (MR), and metabolic activity (MA) were calculated as:

$$MF = \frac{1}{IR \times IZ \times IX_C \times IXL} \quad (25)$$

$$MR = WTR \times NAC \quad (26)$$

$$MA = \sqrt[6]{MF \times MR} \quad (27)$$

where MF is metabolic flow; MR is metabolic rate; MA is metabolic activity; IR, IZ, IX_C, and IX_L are intrinsic resistance, intrinsic impedance, intrinsic capacitive reactance, and intrinsic inductive reactance, respectively; WTR is dynamic water-transfer rate (Equation 13); and NAC is nutrient active translocation capacity (Equation 18).

Correlation analysis and comprehensive evaluation by membership function

Correlation analysis was performed to examine relationships among measured traits and electrophysiological indices. Comprehensive tolerance was evaluated using the membership-function method.

$$U(X_{ij}) = (X_{ij} - X_{jmin}) / (X_{jmax} - X_{jmin}) \quad (28)$$

where X_{ij} is the observed value of index j under treatment i; X_{jmin} and X_{jmax} are the minimum and maximum values of index j across all treatments, respectively; and $U(X_{ij})$ is the normalized membership value. The comprehensive membership value (D) was calculated as the mean of $U(X_{ij})$ across the selected indices.

Data statistics and analysis

Electrophysiological parameter equations were fitted using SigmaPlot 12 (Systat Software, San Jose, California, USA). Statistical analyses were performed using SPSS 21.0 (IBM, Armonk, New York, USA). Treatment effects were evaluated by one-way ANOVA, and mean comparisons were conducted using the least significant difference (LSD) test at $p < 0.05$. Results are presented as mean ± standard deviation (SD), and different letters indicate significant differences among treatments. Correlation heatmaps were generated using OriginPro 2024 (OriginLab Corporation, Northampton, Massachusetts, USA).

RESULTS

Growth parameters

Table 2 presents the growth traits of *P. asiatica* under PE stress across different Se(IV) (sodium selenite) treatments. Crown, TChl, and TN exhibited the same trend: S2 > S3 > S1 > CK > S4. Plant height followed the order: S4 > S3 > S2 > S1 > CK. Notably, S2 resulted in the highest TChl and TN, increasing by 11.84% and 9.30% relative to CK, respectively.

Table 2. Growth parameters of *Plantago asiatica* under polyethylene (PE) stress across different Se(IV) (sodium selenite) treatments. Each value represents mean ± SD. CK: 0 mg kg^{-1} Se(IV); PE-1500 mg kg^{-1}; S1: 1.25 mg kg^{-1} Se(IV); PE-1500 mg kg^{-1}; S2: 2.5 mg kg^{-1} Se(IV); PE-1500 mg kg^{-1}; S3: 12.5 mg kg^{-1} Se(IV); PE-1500 mg kg^{-1}; S4: 25 mg kg^{-1} Se(IV); PE-1500 mg kg^{-1}. TChl: Leaf total chlorophyll content; TN: total N content. Different letters within a given parameter indicate significant differences among treatments ($n = 5$, $p < 0.05$).

Group	CK	S1	S2	S3	S4
Crown, cm	29.61 ± 3.01^{d}	31.78 ± 4.23^{c}	34.57 ± 2.74^{a}	32.56 ± 3.13^{b}	26.86 ± 2.21^{e}
Height, cm	25.45 ± 4.17^{e}	26.14 ± 5.45^{d}	27.15 ± 1.87^{c}	27.33 ± 4.43^{b}	30.82 ± 2.51^{a}
TChl, mg g^{-1}	53.2 ± 1.3^{e}	57.1 ± 2.2^{c}	59.5 ± 2.1^{a}	58.5 ± 1.5^{b}	53.2 ± 0.9^{d}
TN, mg g^{-1}	19.5 ± 0.7^{e}	20.7 ± 0.5^{c}	21.5 ± 0.4^{a}	21.2 ± 0.5^{b}	20.5 ± 0.6^{d}

Photosynthesis

Figure 2 presents photosynthesis data for *P. asiatica* under PE stress with different Se(IV) (sodium selenite) treatments. The P_N (Figure 2a), g_{sw} (Figure 2b), C_i (Figure 2c), and T_r (Figure 2d) showed an initial increase followed by a decline, with the overall pattern S2 > S3 > S1 > S4 > CK. The S2 reached the highest values, exceeding CK by 91.04%, 408.95%, 52.29%, and 241.60%, respectively. By contrast, WUE (Figure 2e) first decreased and then increased, following the order CK > S4 > S1 > S2 > S3, with S3 being the lowest, 51.82% below CK.

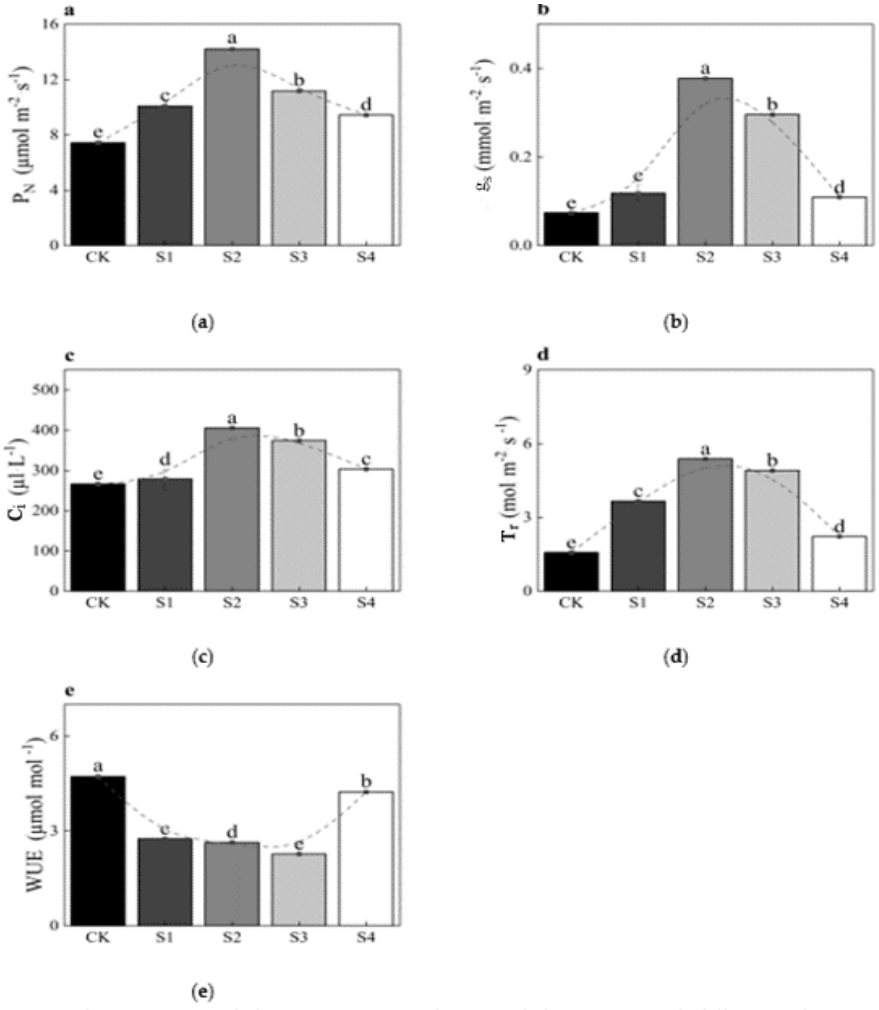

Figure 2. Photosynthesis of *Plantago asiatica* under polyethylene (PE) stress with different Se(IV) (sodium selenite) treatments: Net photosynthetic rate (P_N) (a); stomatal conductance (g_{sw}) (b); intercellular CO_2 concentration (C_i) (c); transpiration rate (T_r) (d); water-use efficiency (WUE) (e). CK: 0 mg kg^{-1} Se(IV); PE-1500 mg kg^{-1}; S1: 1.25 mg kg^{-1} Se(IV); PE-1500 mg kg^{-1}; S2: 2.5 mg kg^{-1} Se(IV); PE-1500 mg kg^{-1}; S3: 12.5 mg kg^{-1} Se(IV); PE-1500 mg kg^{-1}; S4: 25 mg kg^{-1} Se(IV); PE-1500 mg kg^{-1}. Data are presented as mean ± standard deviation; different letters indicate significant differences among treatments.

Intrinsic electrophysiological information of plant leaves

Figure 3 illustrates the intrinsic electrophysiological properties of *P. asiatica* leaves under PE stress across different Se(IV) (sodium selenite) treatments. The ICP (Figure 3a) exhibited an initial increase followed by a decline, with the sequence S2 > S1 > S4 > S3 > CK; S2 reached the maximum, 353.26% higher than CK. The IR (Figure 3b), IZ (Figure 3c), IX_C (Figure 3d), and IX_L (Figure 3e) all decreased initially and then increased, following the order CK > S3 > S4 > S1 > S2.

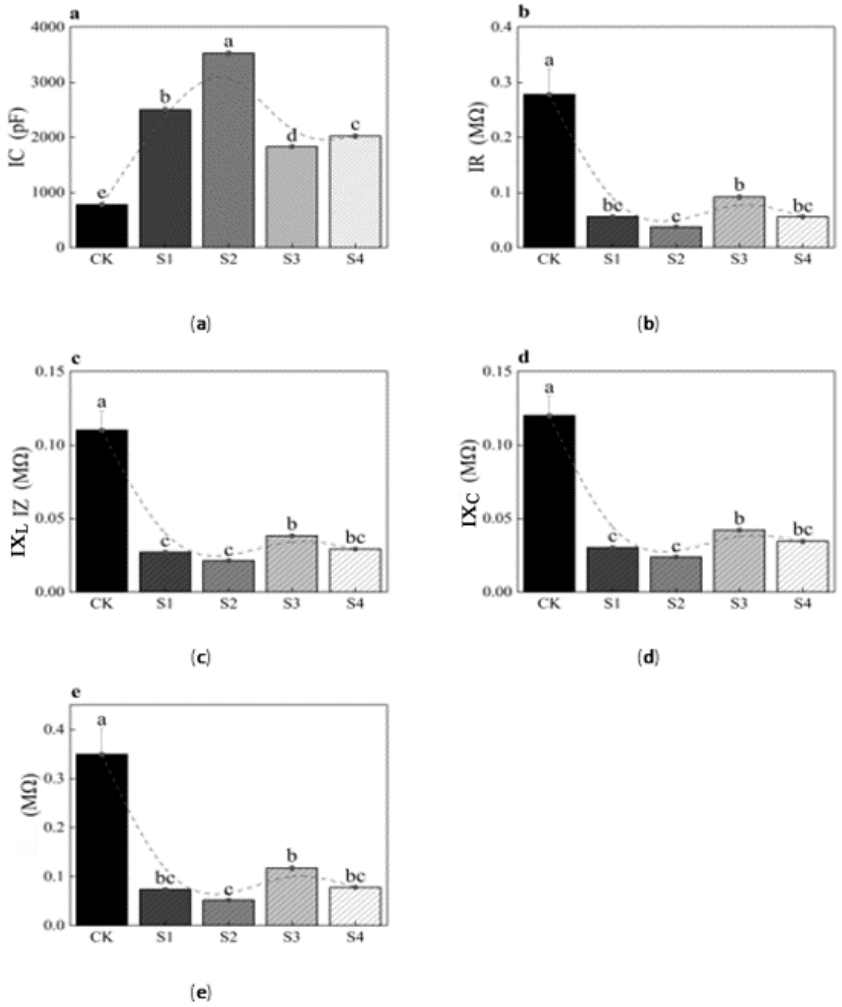

Figure 3. Intrinsic electrophysiological properties of *Plantago asiatica* leaves under polyethylene (PE) stress with different Se(IV) treatments CK: 0 mg kg^{-1} Se(IV); PE-1500 mg kg^{-1}; S1: 1.25 mg kg^{-1} Se(IV); PE-1500 mg kg^{-1}; S2: 2.5 mg kg^{-1} Se(IV); PE-1500 mg kg^{-1}; S3: 12.5 mg kg^{-1} Se(IV); PE-1500 mg kg^{-1}; S4: 25 mg kg^{-1} Se(IV); PE-1500 mg kg^{-1}. ICP: Intrinsic physiological capacitance; IR: intrinsic resistance; IZ: intrinsic impedance; IX_C: intrinsic capacitive reactance; IX_L: intrinsic inductive reactance. Data are presented as mean ± standard deviation; different letters indicate significant differences among treatments.

Cellular water metabolism of leaves

Figure 4 illustrates the intracellular water metabolism of *P. asiatica* leaves under PE stress with different Se(IV) (sodium selenite) treatments. The IWHC (Figure 4a) and WTR (Figure 4d) increased initially and then declined, following the sequence S2 > S1 > S4 > S3 > CK, with S2 reaching the maximum, exceeding CK by 173.95% and 209.15%, respectively. The IWUE (Figure 4b) ranked as CK > S1 > S3 > S2 > S4, with S4 being the lowest, 50.52% below CK. The IWHT (Figure 4c) followed CK > S2 > S3 > S1 > S4, with S4 being the minimum, 30.69% lower than CK.

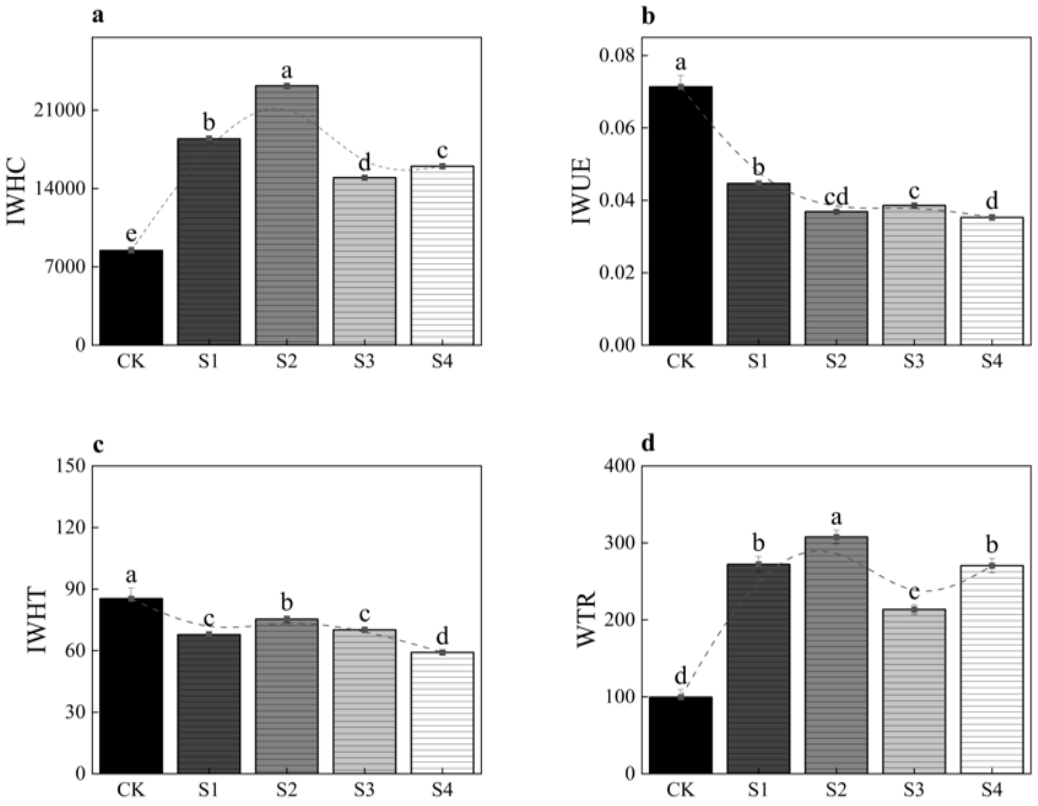

Figure 4. Intracellular water metabolism characteristics of *Plantago asiatica* leaves under polyethylene (PE) stress with different Se(IV) (sodium selenite) treatments: Intracellular water-holding capacity (IWHC) (a); intracellular water use efficiency (IWUE) (b); intracellular water holding time (IWHT) (c); intracellular water transfer rate (WTR) (d). CK: 0 mg kg^{-1} Se(IV); PE-1500 mg kg^{-1}; S1: 1.25 mg kg^{-1} Se(IV); PE-1500 mg kg^{-1}; S2: 2.5 mg kg^{-1} Se(IV); PE-1500 mg kg^{-1}; S3: 12.5 mg kg^{-1} Se(IV); PE-1500 mg kg^{-1}; S4: 25 mg kg^{-1} Se(IV); PE-1500 mg kg^{-1}. Data are presented as mean ± standard deviation; different letters indicate significant differences among treatments.

Nutrient transport characteristics in leaf cells

Figure 5 depicts the intracellular nutrient translocation characteristics of *P. asiatica* leaves under PE stress with different Se(IV) (sodium selenite) treatments. The UNF (Figure 5a) followed the order CK > S3 > S1 > S2 (S4), with S2 and S4 being the lowest, each 25.93% below CK; NTR (Figure 5b) ranked as S2 > S1 (S4) > S3 > CK, with S2 being the highest, 109.15% above CK; NTC (Figure 5c) followed S1 > S2 > S3 (S4) > CK, with S1 being the maximum, 131.94% higher than CK. Both UAF (Figure 5d) and NAC (Figure 5e) showed the pattern S2 > S4 > S1 > S3 > CK, with S2 reaching the highest values, exceeding CK by 33.41% and 311.29%, respectively.

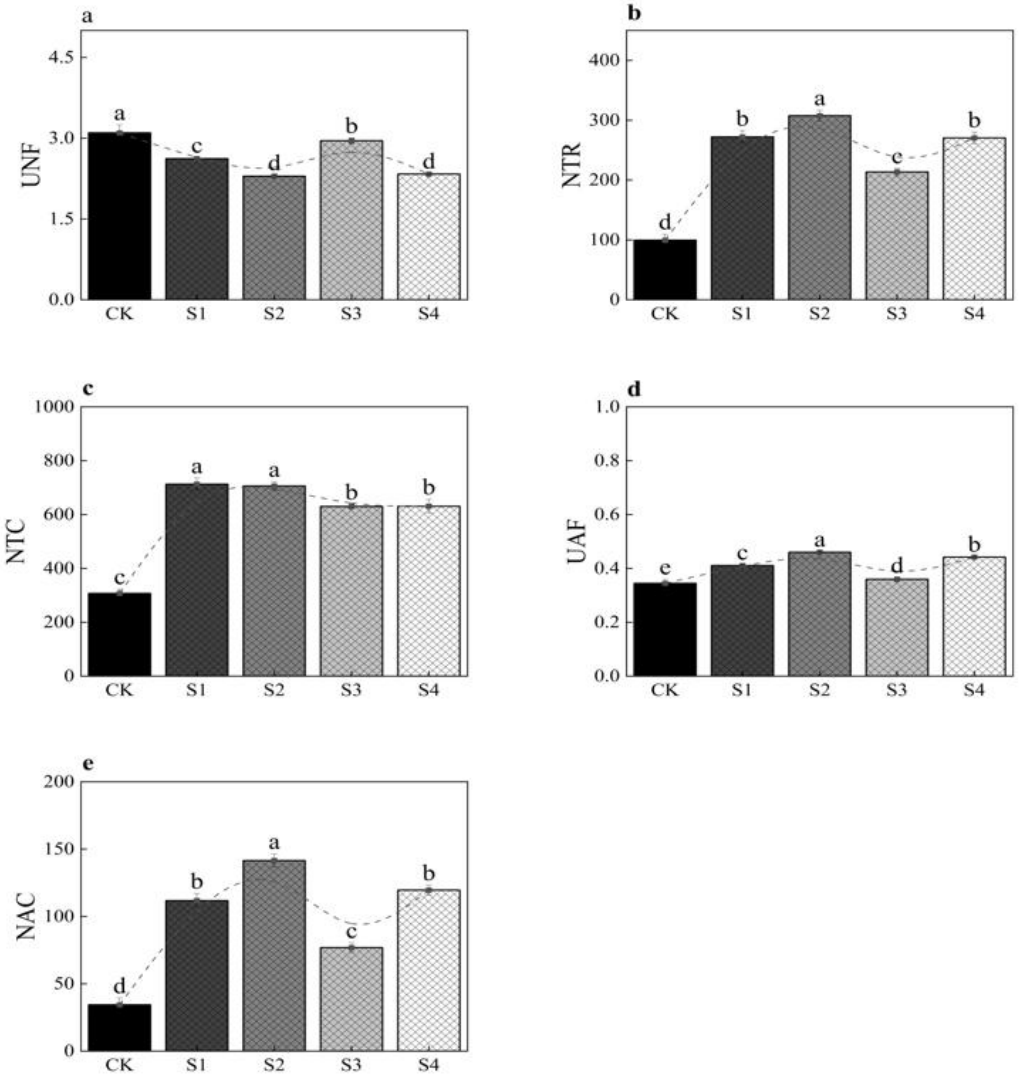

Figure 5. Intracellular nutrient translocation characteristics of *Plantago asiatica* leaves under polyethylene (PE) stress with different Se(IV) (sodium selenite) treatments: Nutrient flux per unit area (UNF) (a); nutrient transfer rate (NTR) (b); nutrient translocation capacity (NTC) (c); active transport flow of nutrient (UAF) (d); nutrient active translocation capacity (NAC) (e). CK: 0 mg kg^{-1} Se(IV); PE-1500 mg kg^{-1}; S1: 1.25 mg kg^{-1} Se(IV); PE-1500 mg kg^{-1}; S2: 2.5 mg kg^{-1} Se(IV); PE-1500 mg kg^{-1}; S3: 12.5 mg kg^{-1} Se(IV); PE-1500 mg kg^{-1}; S4: 25 mg kg^{-1} Se(IV); PE-1500 mg kg^{-1}. Data are presented as mean ± standard deviation; different letters indicate significant differences among treatments.

Cellular metabolic energy of leaves

Table 3 presents the cellular metabolic energy of *P. asiatica* leaves under PE stress across different Se(IV) (sodium selenite) treatments. The ΔG_{LE} followed the order: CK > S2 > S1 > S3 > S4, with S4 being the lowest, 31.78% below CK; ΔG_L ranked as S2 > S1 > CK > S3 > S4, with S2 being the highest, 38.46% above CK.

Table 3. Cellular metabolic energy of *Plantago asiatica* leaves under polyethylene (PE) stress with different Se(IV) treatments. CK: 0 mg kg^{-1} Se(IV); PE-1500 mg kg^{-1}; S1: 1.25 mg kg^{-1} Se(IV); PE-1500 mg kg^{-1}; S2: 2.5 mg kg^{-1} Se(IV); PE-1500 mg kg^{-1}; S3: 12.5 mg kg^{-1} Se(IV); PE-1500 mg kg^{-1}; S4: 25 mg kg-1 Se(IV); PE-1500 mg kg-1. $\triangle G_{LE}$: Total cellular metabolic energy of plant leaves; $\triangle G_L$: total cellular metabolic energy. Data are presented as mean ± standard deviation; different letters indicate significant differences among treatments.

Group	CK	S1	S2	S3	S4
$\triangle G_{LE}$	2.06 ± 0.0051^{a}	1.59 ± 0.032^{b}	1.61 ± 0.02^{b}	1.50 ± 0.00^{c}	0.99 ± 0.04^{d}
$\triangle G_L$	1245.68 ± 5.43^{c}	1311.29 ± 29.52^{b}	1381.68 ± 26.56^{a}	870.35 ± 3.33^{d}	561.88 ± 30.25^{e}

Metabolic flow of leaf cells

Figure 6 presents the cellular metabolic flow of *Plantago asiatica* leaves under PE stress with different Se(IV) (sodium selenite) treatments. The MF (Figure 6a), MR (Figure 6b), and MA (Figure 6c) all followed the order: S2 > S1 > S4 > S3 > CK, with S2 reaching the highest values, exceeding CK by 244.29%, 1103.99%, and 24.73%, respectively.

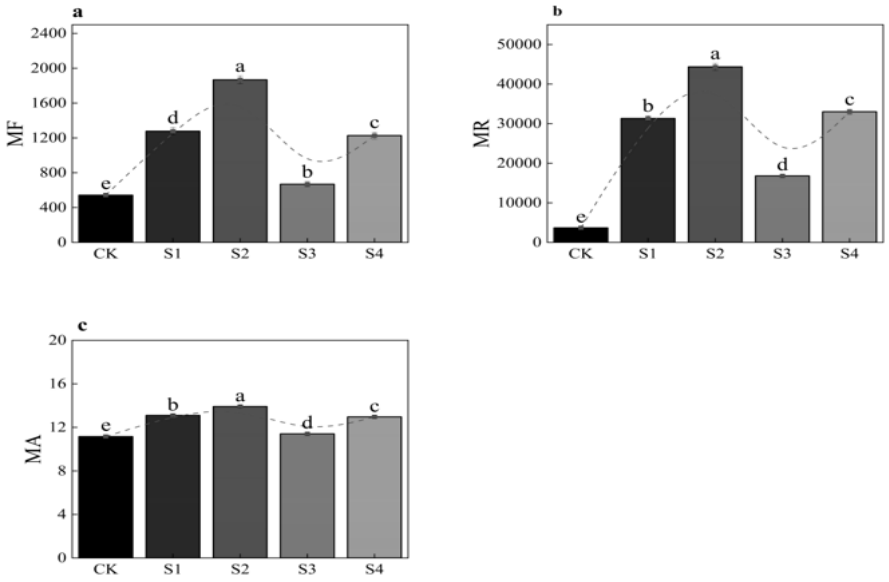

Figure 6. Leaf cellular Metabolic flow of *Plantago asiatica* under polyethylene (PE) stress with different Se(IV) (sodium selenite) treatments: Metabolic flow (MF) (a); metabolic rate (MR) (b); metabolic activity (MA) (c). CK: 0 mg kg^{-1} Se(IV); PE-1500 mg kg^{-1}; S1: 1.25 mg kg^{-1} Se(IV); PE-1500 mg kg^{-1}; S2: 2.5 mg kg^{-1} Se(IV); PE-1500 mg kg^{-1}; S3: 12.5 mg kg^{-1} Se(IV); PE-1500 mg kg^{-1}; S4: 25 mg kg^{-1} Se(IV); PE-1500 mg kg^{-1}. Data are presented as mean ± standard deviation; different letters denote significant differences among treatments.

Correlation analysis and membership function ordering

Figure 7 presents the correlation analysis of growth, photosynthesis, and leaf intracellular nutrient metabolism features of *P. asiatica* under PE stress with different Se(IV) (sodium selenite) treatments. Growth showed significant positive correlations with TChl, TN, P_N, g_{sw}, C_i, T_r, IWHC, NTC, and MA, and significant negative correlations with WUE and IWUE. Based on the significant difference indices in Figure 7, the variables were ranked using the membership function method (Table 4). The results indicate that S2 is the optimal Se(IV) concentration for *P. asiatica* under PE stress, yielding the highest membership values for photosynthesis and IWHC, together with strong nutrient-transport performance.

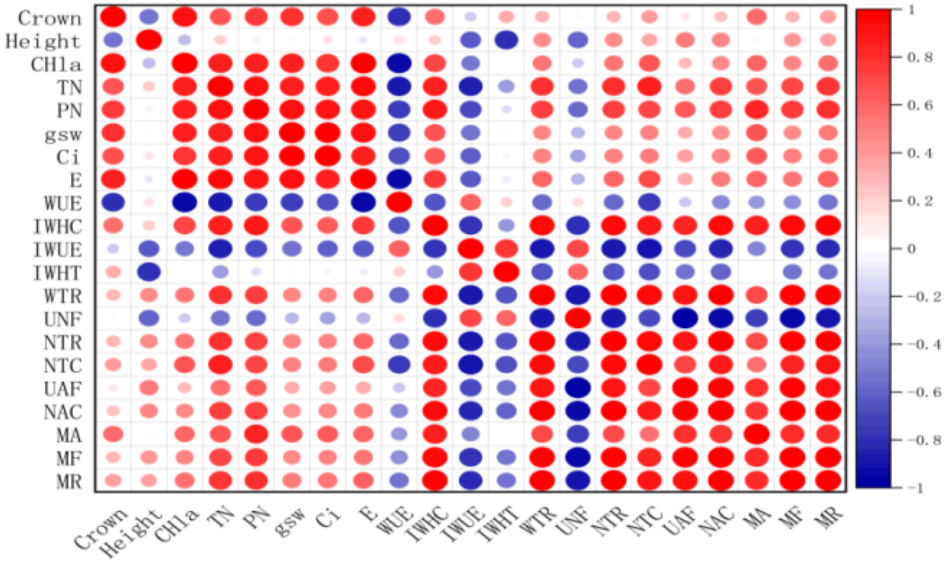

Figure 7. Correlation analysis of growth, photosynthesis, and leaf intracellular nutrient metabolism features of *Plantago asiatica* under polyethylene (PE) stress with different Se(IV) (sodium selenite) treatments. Crown: Crown width; Height: plant height; TChl: total chlorophyll; TN: total N; PN: net photosynthetic rate; g_{sw}: stomatal conductance; C_i: intercellular CO_2 concentration; T_r: transpiration rate; WUE: water-use efficiency; IWHC: intracellular water-holding capacity; IWUE: intracellular water-use efficiency; IWHT: intracellular water-holding time; WTR: leaf intracellular water transfer rate; UNF: nutrient flux per unit area; NTR: nutrient transfer rate; NTC: nutrient translocation capacity; UAF: active transport flow of nutrient; NAC: nutrient active translocation capacity; MA: relative metabolic activity; MF: leaf metabolic flow; MR: leaf metabolic rate.

Table 4. Membership function values for *Plantago asiatica* growth, photosynthesis, and leaf intracellular nutrient metabolism features exhibiting significant differences under polyethylene (PE) stress with different Se(IV) treatments. CK: 0 mg kg^{-1} Se(IV); PE-1500 mg kg^{-1}; S1: 1.25 mg kg^{-1} Se(IV); PE-1500 mg kg^{-1}; S2: 2.5 mg kg^{-1} Se(IV); PE-1500 mg kg^{-1}; S3: 12.5 mg kg^{-1} Se(IV); PE-1500 mg kg^{-1}; S4: 25 mg kg^{-1} Se(IV); PE-1500 mg kg^{-1}. TChl: Chlorophyll (mg g^{-1}); P_N: net photosynthetic rate (μmol $m^{-2}·s^{-1}$); g_{sw}: stomatal conductance (mmol $m^{-2}·s^{-1}$); IWHC: intracellular water-holding capacity; NTC: nutrient translocation capacity.

Group (×10^{-2})	CK	S1	S2	S3	S4
UChl	0	61.9	100	84.13	0.00
UC_i	0	8.69	100	77.17	26.41
UWUE	100	19.59	15.10	0.00	80.00
UMA	1.17	0.00	0	100.00	0.00
UHeight	0	12.84	31.67	35.01	100.00
UP_N	0	39.12	100	55.20	29.54
UE	0	55.00	100	87.90	17.11
Ug_{sw}	0	13.33	100	73.33	10.00
UIWHC	0	59.58	100	50.86	56.96
UNTC	0	99.92	98.21	79.47	79.63
Average value	10.12	37.11	74.51	64.31	37.96
Ranking	5	4	1	2	3

DISCUSSION

Se(IV) enhanced leaf intrinsic physiological capacitance (ICP) to alleviate polyethylene inhibition of plantain growth

Moderate Se(IV) concentrations help alleviate polyethylene (PE) stress, whereas excessive Se(IV) hampers plant growth (Hasanuzzaman et al., 2020). In the present study, 2.5 mg kg^{-1} Se(IV) (S2) significantly alleviated growth stress in plantain (*Plantago asiatica* L.), while concentrations above 2.5 mg kg^{-1} Se(IV) inhibited growth. Under S2, Crown, leaf total chlorophyll (TChl), and total N (TN) reached their peaks, all of which declined when Se(IV) concentrations exceeded 2.5 mg kg^{-1}. The Se(IV) has been shown to promote chlorophyll synthesis, enhance photosynthesis, and supply additional nutrients for plant growth (Pilon-Smits, 2019). It also facilitates N uptake, reducing pollutant accumulation and toxicity (Bhadwal and Sharma, 2022). Previous research has confirmed that various metal ions and nutritional states influence intrinsic leaf electrophysiological parameters (Qin et al., 2022).

In this study, leaf intrinsic physiological capacitance (ICP) (Figure 3) mirrored trends observed in growth (Table 2) and photosynthesis (Figure 2), with the highest ICP observed under S2, indicating that 2.5 mg kg^{-1} Se(IV) promoted leaf capacitance. Earlier studies have shown a significant positive correlation between ICP and plant growth; within nutrient thresholds conducive to growth, the vacuole volume of mesophyll cells increases, enhancing the efficiency of water and nutrient accumulation and translocation, which in turn elevates leaf capacitance (Zhang et al., 2020). Simultaneously, intrinsic resistance (IR), intrinsic impedance (IZ), intrinsic capacitive reactance (IX_C), and intrinsic inductive reactance (IX_L) under S2 were inversely correlated with growth, showing minimal values at S2. These results suggest better growth status and an increased nutrient translocation rate (NTR) across the mesophyll cell wall and membrane, reflected in reduced physiological resistance and impedance of mesophyll cells, consistent with previous findings (Hasanuzzaman et al., 2022). In contrast, when Se(IV) concentrations exceeded 2.5 mg kg^{-1}, growth was inhibited, ICP decreased, and IR, IZ, IX_C, and IX_L increased, indicating that excessive Se(IV) reduced the NTR in mesophyll cells, in agreement with the literature (Hasanuzzaman et al., 2020).

Se(IV) enhances active transport of intracellular nutrients in leaves of plantain to reduce stress

Building on the intrinsic electrophysiological features of *P. asiatica* leaves (ICP, IR, IZ, IX_C, and IX_L), intracellular nutrient metabolism was quantified, including water metabolism (Figure 4) and nutrient translocation (Figure 5). It was observed that, with increasing Se(IV) concentration, intracellular water-holding capacity (IWHC) and dynamic water-transfer rate (WTR) peaked under S2, while intracellular water-use efficiency (IWUE) and relative water-holding time (IWHT) declined (Figure 4). The S2 was the optimal Se(IV) concentration for growth, suggesting that intracellular nutrient translocation metabolism was enhanced under this condition. Previous studies have shown that Se(IV) promotes intracellular water translocation in leaves, thereby mitigating stress (Zhang et al., 2021). In our experiment, 2.5 mg kg^{-1} Se(IV) increased leaf total chlorophyll (TChl) and enhanced photosynthesis, which improved the efficiency of intracellular water translocation and reduced water-holding time. Concurrently, 2.5 mg kg^{-1} Se(IV) promoted growth and facilitated water accumulation in mesophyll cells, reflected in an increased intracellular water-holding capacity (IWHC). Additionally, Se(IV) can elevate leaf stomatal conductance and transpiration rate, which reduces the intracellular water-use rate—consistent with the behavior of instantaneous water-use efficiency (WUE) (Hasanuzzaman et al., 2020). Consequently, the intracellular water-use efficiency (IWUE) under S2 was lower. However, when Se(IV) concentrations exceeded 2.5 mg kg^{-1}, IWHC and dynamic water-transfer rate (WTR) declined, while IWUE and relative water-holding time (IWHT) increased, likely due to the combined inhibitory effects of excessive Se(IV) and polyethylene (PE) on growth, which reduced intracellular nutrient translocation capacity (NTC). In response, leaf cells extended IWHT and improved water-use efficiency to mitigate growth stress, consistent with previous findings (Azizi et al., 2014).

Notably, S2 exhibited the strongest overall active-transport performance, with the highest nutrient translocation rate (NTR) and nutrient active translocation capacity (NAC) and a consistently high nutrient transport capacity (NTC) (Figure 5). This may be attributed to S2 promoting the expression of Se(IV) transporters. For instance, Se(IV) enhances the expression of rice OsNIP2;1 (Chang et al., 2019) and tea-leaf CsNIP2;1 (Cao et al., 2021), thereby improving nutrient translocation efficiency. Furthermore, since S2 promoted growth, it is suggested that Se(IV), water, and other nutrients across the cell membrane reached a transmembrane transport equilibrium, reducing the concentration gradient caused by free diffusion (Ismael et

al., 2019). Simultaneously, intracellular synthetic products under S2, such as total chlorophyll (TChl) and total N (TN), increased. These processes depend on active transport within leaf cells, which provides carriers and energy. In this study, S2 reduced nutrient loss from leaf cells, as indicated by a lower nutrient unit flow (UNF). In contrast, when Se(IV) concentrations exceeded 2.5 mg kg^{-1}, active transport diminished, and free diffusion increased, resulting in decreases in NTR, NTC, and NAC, along with an elevated UNF. This outcome likely reflects the exacerbated oxidative stress in leaves caused by excessive Se(IV) and PE, which suppresses the active translocation of intracellular nutrients and aggravates cellular nutrient loss (Jomova et al., 2024).

Se(IV) promotes mesophyll cell metabolic energy and enhances its resistance to PE

Building on the intracellular water and nutrient metabolism features outlined above, cellular metabolic energy ($\triangle G_L$) and metabolic flow (MF) were used to assess *P. asiatica*'s ability to withstand PE stress. The results showed that $\triangle G_L$ (Table 3) and metabolic activity (MA) (Figure 6) were highest under S2, indicating that 2.5 mg kg^{-1} Se(IV) is the optimal Se(IV) concentration for enhancing resistance to PE stress in *P. asiatica*. The S2 increased leaf IWHC and NTC (Jócsák et al., 2019), thereby promoting cellular metabolic energy. Under S2, IWUE and free diffusion were reduced, which decreased intracellular nutrient loss and alleviated PE stress (Jócsák et al., 2019). Moreover, Se(IV) in S2 may have enhanced antioxidant enzyme activities, such as selenomethionine (Se-Met) (Yuan et al., 2024), glutathione peroxidase (GPX) (Yuan et al., 2024), and thioredoxin reductase (TrxR) (Yuan et al., 2024), thereby reducing reactive oxygen species (ROS) damage and promoting cellular metabolism under S2. In contrast, Se(IV) levels exceeding 2.5 mg kg^{-1}, combined with PE stress, likely intensified oxidative stress in *P. asiatica* leaves (Yuan et al., 2024), leading to decreased cellular metabolic energy.

Electrophysiological characteristics of leaves reveal the mechanism of Se(IV) alleviating PE in plant nutrition and metabolism

In this experiment, IWHC, NTC, and MA were identified as key electrophysiological indicators for evaluating how different Se(IV) treatments alleviate PE stress in *P. asiatica*. Based on correlation analysis (Qin et al., 2022), it was found that, under PE stress, growth showed significant positive correlations with TChl, TN, net photosynthetic rate (P_N), stomatal conductance(g_{sw}), intercellular CO_2 concentration (C_i), transpiration rate (T_r), IWHC, NTC, and MA, and significant negative correlations with WUE and IWUE (Figure 7). These results indicate that Se(IV) mitigates PE stress by enhancing intracellular water transfer and active nutrient translocation while reducing intracellular water-use efficiency. Using a comprehensive evaluation via the membership function (Qin et al., 2022), S2 (2.5 mg kg^{-1} Se(IV)) was identified as the optimal Se(IV) concentration for mitigating PE stress in *P. asiatica*, as evidenced by the highest values of IWHC and MA under S2, together with strong nutrient-transport performance (Table 4). When Se(IV) exceeded 2.5 mg kg^{-1}, leaf IWHC, NTC, and MA decreased, suggesting that both Se(IV) and PE jointly suppressed plant growth.

CONCLUSIONS

In summary, this experiment screened electrophysiological indicators—specifically intracellular water-holding capacity (IWHC), nutrient translocation capacity (NTC), and metabolic activity (MA)—to elucidate the mechanisms by which different Se(IV) treatments alleviate polyethylene (PE) stress in *Plantago asiatica*. The results indicate that 2.5 mg kg^{-1} Se(IV) is the optimal Se(IV) concentration for mitigating PE stress. Under S2, IWHC and MA increased markedly, while nutrient transport remained strong, thereby improving intracellular water regulation and active nutrient transport and alleviating PE stress. When Se(IV) exceeded 2.5 mg kg^{-1}, both Se(IV) and PE suppressed plant growth, with reductions in IWHC, NTC, and MA, as well as a decline in leaf IWHC and active nutrient transport. In conclusion, plant electrophysiological technology offers a novel approach for online monitoring of Se(IV)-mediated mitigation of *P. asiatica* PE stress, providing a strong foundation for the development of agricultural Se health.

Author contribution

Conceptualization: H.M. Methodology: Y.W. Formal analysis: H.M. Investigation: H.M. Data curation: A.X., Y.W. Writing-original draft: H.M. Writing-review & editing: Y.W., J.W. Supervision: X.C., A.X. Project administration: A.X. Funding acquisition: A.X. All co-authors reviewed the final version and approved the manuscript before submission.

Acknowledgements

This research was funded by the Guizhou Provincial Science and Technology Program (Qiankehe Foundation–ZK[2024] General 433).

References

Azizi, T., Saidi, W., Rezgui, M., Mechri, M., Melki, M. 2014. Periodic variation of the water use efficiency in durum wheat. Pakistan Journal of Biological Sciences 17(11):1141-1151. doi:10.3923/pjbs.2014.1141.1151

Bhadwal, S., Sharma, S. 2022. Selenium alleviates physiological traits, nutrient uptake and nitrogen metabolism in rice under arsenate stress. Environmental Science and Pollution Research 29(47):70862-70871. doi:10.1007/s11356-022-20762-5.

Brown, P.H., Zhao, F.J., Dobermann, A. 2022. What is a plant nutrient? Changing definitions to advance science and innovation in plant nutrition. Plant and Soil 47:11-23. doi:10.1007/s11104-021-05171-w.

Cao, D., Liu, Y., Ma, L., Liu, Z., Li, J., Wen, B., et al. 2021. Genome-wide identification and characterization of phosphate transporter gene family members in tea plants (*Camellia sinensis* L. O. Kuntze) under different selenite levels. Plant Physiology and Biochemistry 166:668-676. doi:10.1016/j.plaphy.2021.06.038.

Chang, C., Yin, R., Wang, X., Shao, S., Chen, C., Zhang, H. 2019. Selenium translocation in the soil-rice system in the Enshi seleniferous area, Central China. Science of the Total Environment 669:83-90.

Hasanuzzaman, M., Bhuyan, M.H.M.B., Raza, A., Hawrylak-Nowak, B., Matraszek-Gawron, R., Nahar, K., et al. 2020. Selenium toxicity in plants and environment: Biogeochemistry and remediation possibilities. Plants 9(12):1711. doi:10.3390/plants9121711.

Hasanuzzaman, M., Nahar, K., García-Caparrós, P., Parvin, K., Zulfiqar, F., Ahmed, N., et al. 2022. Selenium supplementation and crop plant tolerance to metal/metalloid toxicity. Frontiers in Plant Science 12:792770. doi:10.3389/fpls.2021.792770.

Ismael, M.A., Elyamine, A.M., Moussa, M.G., Cai, M., Zhao, X., Hu, C. 2019. Cadmium in plants: uptake, toxicity, and its interactions with selenium fertilizers. Metallomics 11(2):255-277. doi:10.1039/C8MT00247A.

Jócsák, I., Végvári, G., Vozáry, E. 2019. Electrical impedance measurement on plants: A review with some insights to other fields. Theoretical and Experimental Plant Physiology 31(3):317-330. doi:10.1007/s40626-019-00152-y.

Jomova, K., Alomar, S.Y., Alwasel, S.H., Nepovimova, E., Kuca, K., Valko, M. 2024. Several lines of antioxidant defense against oxidative stress: antioxidant enzymes, nanozymes and low-molecular-weight antioxidants. Archives of Toxicology 98(5):1323-1367. doi:10.1007/s00204-024-03696-4.

Kulbacka, J., Choromańska, A., Rossowska, J., Wezgowiec, J., Saczko, J., Rols, M-P. 2018. Cell membrane transport mechanisms: Ion channels and electrical properties of cell membranes. p. 39-58. In Kulbacka, J., Satkauskas, S. (eds.) Transport across natural and modified biological membranes and its implications in physiology and therapy. Springer, Cham, Switzerland. doi:10.1007/978-3-319-56895-9.

Li, J.H., Fan, L.F., Zhao, D.J., Zhou, Q., Yao, J.P., Wang, Z.Y. 2021. Plant electrical signals: A multidisciplinary challenge. Journal of Plant Physiology 261:153418. doi:10.1016/j.jplph.2021.153418.

Li, J., Yu, S., Yu, Y., Xu, M. 2022. Effects of microplastics on higher plants: A review. Bulletin of Environmental Contamination and Toxicology 109:241-265. doi:10.1007/s00128-022-03566-8.

Liu, K., Zhang, B.L., Zhang, W.Y., Zhang, Y.B., Tian, X.H. 2018. Application of non-invasive microelectrode ion flux estimation technique in crop stress physiology. Ying Yong Sheng Tai Xue Bao 29(2):678-686.

Pilon-Smits, E.A. 2019. On the ecology of selenium accumulation in plants. Plants 8(7):197. doi:10.3390/plants8070197.

Qin, X., Xing, D., Wu, Y., Wang, W., Li, M., Solangi, K. 2022. Diurnal variation in transport and use of intracellular leaf water and related photosynthesis in three karst plants. Agronomy 12(11):2758. doi:10.3390/agronomy12112758.

Qiu, G., Han, Z., Wang, Q., Wang, T., Sun, Z., Yu, Y., et al. 2023. Toxicity effects of nanoplastics on soybean (*Glycine max* L.): Mechanisms and transcriptomic analysis. Chemosphere 313:137571. doi:10.1016/j.chemosphere.2022.137571.

Rajput, V.D., Minkina, T., Feizi, M., Kumari, A., Khan, M., Mandzhieva, S., et al. 2021. Effects of silicon and silicon-based nanoparticles on rhizosphere microbiome, plant stress and growth. Biology 10(8):791. doi:10.3390/biology10080791.

Shah, T., Khan, Z., Asad, M., D'amato, R., Alsahli, A.A., Ahmad, P. 2024. Synthetic bacterial community derived from *Astragalus mongholicus* and plant-plant interactions inhibit cadmium uptake under cadmium-contaminated soil. Journal of Environmental Chemical Engineering 12(1):111619. doi:10.1016/j.jece.2023.111619.

Yuan, Z., Cai, S., Yan, C., Rao, S., Cheng, S., Xu, F. 2024. Research progress on the physiological mechanism by which selenium alleviates heavy metal stress in plants: a review. Agronomy 14(8):1787.

Zhang, C., Wu, Y., Su, Y., Li, H., Fang, L., Xing, D. 2021. Plant's electrophysiological information manifests the composition and nutrient transport characteristics of membrane proteins. Plant Signaling & Behavior 16(7):e1918867. doi:10.1080/15592324.2021.1918867.

Zhang, C., Wu, Y.Y., Su, Y., Xing, D., Dai, Y., Wu, Y.S. 2020. A plant's electrical parameters indicate its physiological state: a study of intracellular water metabolism. Plants 9(10):1256. doi:10.3390/plants9101256.